JOURNAL OF MATERIALS SCIENCE 21 (1986) 4081–4088

Predicting failure from the initiation stage of slow crack growth in polyethylene

XICI LU*, NORMAN BROWN
Department of Materials Science and Engineering, University of Pennsylvania, Philadelphia, Pennsylvania 19104, USA

The crack opening displacement against time was measured in linear polyethylene as a function of stress, notch depth, and temperature for three-point bending under plane strain conditions. The experimental conditions were accurately controlled so that the scatter in the rate of damage was within ±20%. Microscopic observations showed that the shape of the damaged zone was triangular for stresses less than one-half the yield point and that the length was predictable from measurements of the crack opening displacement. The initial rate of damage prior to crack growth was constant up to crack opening displacement = 15 to 25 μm. The entire shape of the crack opening displacement–time curve and the time to complete failure could be predicted from the initial damage rate. A theory based on the observed microcrazing is presented which explains the dependence of damage rate on stress intensity and microstructural parameters.

1. Introduction

One purpose of this paper is to show that failure time can be predicted from the initial conditions for slow crack growth. The initial conditions were controlled with a very high degree of accuracy with respect to stress, notch depth, and temperature. Thus a meaningful comparison between the experimental values of failure time and the theoretical values could be obtained. Whereas in most other laboratories failure time and crack growth rates often scatter as much as ±100%, in this investigation the scatter was reduced to ±20%.

Our highly accurate equations for the rate of initiation of crack growth form a reliable experimental basis for the development of theoretical models of crack growth based on micromechanics. In this paper a model for crack growth is presented which is based on our phenomenological equations in combination with microscopic observations of the damage process. Bhattacharya and Brown [1, 2] have presented the microstructural features of the initial damaged zone in polyethylene.

A previous paper by Lu and Brown [3] on single edge notched tensile specimens is similar to this investigation which involves notched three-point bending specimens. There is general agreement between the results of both types of experiments. However, for a given stress intensity the rate of damage in three-point bending is significantly lower than for a single edge notched tensile specimen. This difference arises from the non-linear elastic behaviour of PE.

2. Experimental details

The resin was Marlex 6006 produced by the Phillips Chemical Company. It is a linear polymer with melt index of 0.75, M_n = 19 600, M_w = 130 000. After compression moulding the density was 0.964 g cm^{-3}. The yield point at 300 K and at a strain rate of 0.02 min^{-1} is 25 MPa.

The method of compression moulding was recommended by van Dijk [4] who found that the following procedure greatly reduced the scatter in the experimental data on slow crack growth. The compression die is a square chamber 16 cm × 16 cm and 18 mm deep with a close fitting piston. When the polymer is in the range of temperature from about 150 to 180° C, a pressure of about 6.6 MPa is alternately exerted and released for about 6 cycles. Finally the melt is solidified under a pressure of 1.7 MPa and slowly cooled overnight. This pressurizing and depressurizing process supposedly tends to eliminate voids in the melt.

The compression moulded plaques were generally about 4.25 mm thick although some thicker specimens were also tested. The dimensions of the three point bending specimens are shown in Fig. 1.

Controlling the uniformity and depth of the notch is the most critical factor for obtaining reproducible data. A special notching device was designed for producing notch depths with a razor blade. The notch depth was usually controlled to less than ±10 μm. The actual notch depth was measured within ±2 μm. The results on specimens with about the same notch depth could be normalized to a common notch depth within ±2 μm.

The specimens were loaded in three-point bending with a lever loaded apparatus. Positioning the specimen within the loading jig was carefully controlled. The total uncertainties in specimen dimensions made

Present address: University of Science and Technology of China, Hefei, Anhui, People's Republic of China.

0022–2461/86 $03.00 + .12

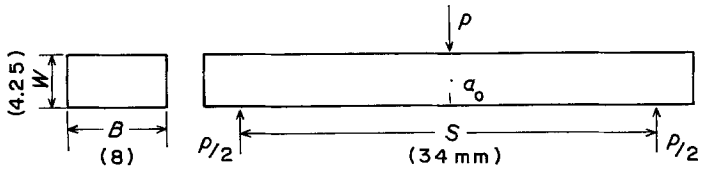

Figure 1 Three-point bending specimens.

the major contribution to the 5% scatter in the outer fibre stress. The temperature of the specimen in air during the test varied $\pm 0.5°$ C.

The measurements of the notch opening were made at 200 magnification using a filar eyepiece. The opening of the notch at the surface of the specimen and at the root of the original notch were measured as a function of time. The error in the measurement of the notch opening was $\pm 2\,\mu$m.

The applied stresses were below one-half the yield point because previous work [2] showed that the higher stresses changed the fracture mechanism by producing a balloon shape damage zone instead of a wedged shape damage zone which is characteristic of long time brittle failure in PE.

The damaged zone was observed in the SEM in a special jig in which the notch opening could be made equal to that which existed during the bending test.

3. Results

3.1. Notch angle (α)

Fig. 2 shows typical results for both the opening of the notch at the surface, δ_s, and the crack opening displacement (COD) at the root of the original notch, δ, against time. $(\delta_s - \delta)$ is nearly constant during most of the lifetime of the specimen. The increase in $(\delta_s - \delta)$ begins gradually when the curves begin to accelerate. SEM observations of the notch (Fig. 3) show that the damaged zone is nearly triangular so that the notch angle, α is given by

$$\tan \alpha/2 = \frac{(\delta_s - \delta)/2}{a_0} \quad (1)$$

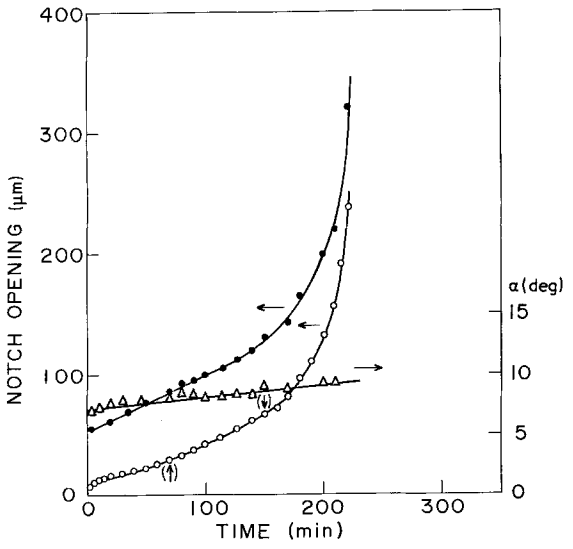

Figure 2 Notch-opening at surface = δ_s (●); opening at root = COD = δ (○), and angle of damage zone α(Δ) against time. a_0 = notch depth of 0.40 mm. The position of arrow (↑) shows the fibrils at the bottom of notch beginning to break, (↓) shows the all fibrils have broken at bottom of notch. Temperature = 42° C.

where a_0 is the depth of the notch. Generally the initial value of α was about 7 and gradually increased to 9° for δ values up to about 150 μm; thereafter it increased rapidly. Thus, for purpose of subsequent calculations, α was taken to be equal to 8°.

Since the shape of the damaged zone was generally a triangular extension of the original notch, up to δ values of about 200 μm, the length of the damaged zone, Δa, is given by

$$\Delta a = \delta/\alpha \quad (2)$$

Equation 2 was confirmed by microscopic measurements of δ and Δa. For δ beyond about 200 μm the boundary of the damaged zone tends to become non-planar when the ligament stress exceeds one-half the yield point.

3.2. Typical δ–t behaviour

Figs 4, 5 and 6 show representative curves of δ–t with stress, σ, notch depth, a_0 and temperature, T, as variables. All curves show the same general behaviour. Shortly after the loading the value of the COD, δ_0, is closely predicted by the Dugdale equation where for plane strain

$$\delta_0 = \frac{K^2}{\sigma_y E(1 - \nu^2)} \quad (3)$$

where K is stress intensity, E is modulus, σ_y is yield point, and ν is Poisson's ratio. The yield point and modulus must be adjusted to take into account temperature and strain rate effects. Recent work by Melve [5] indicates that a value of 0.43 for ν may be appropriate.

Generally the initial slope of the δ–t curve, $\dot{\delta}_0$, is practically constant up to a δ value between 15 to 25 μm. This critical value of δ is called δ_c. At δ_c fibrils begin to break at the bottom of the notch. In Figs 4 to 6, (↑) indicates the beginning and (↓) indicates the completion of fibril fracture at the bottom of the initial notch. δ_c increases somewhat with increasing stress, notch depth, and temperature. Beyond δ_c, the curve begins to accelerate and the SEM micrographs show that the damaged zone then begins to exhibit a true increase in the crack length. Before δ_c, the damaged zone consists of an array of microvoids and fibrils. For δ values above about 200 μm the triangular damaged zone tends to become balloon-like.

3.3. Scatter in the results

Table I shows the reproductibility of the experiments and the scatter in the experimental value of $\dot{\delta}_0$, the initial slope of the δ–t curve. The observed value of $\dot{\delta}_0$ can be normalized to a common value of K by using the Equation 8, i.e. the dependence of $\dot{\delta}_0$ on K_0. The average reproducibility for $\dot{\delta}_0$ is $\pm 14\%$ for the original data and $\pm 9\%$ for the normalized data. This scatter is probably much less than that for any data on slow

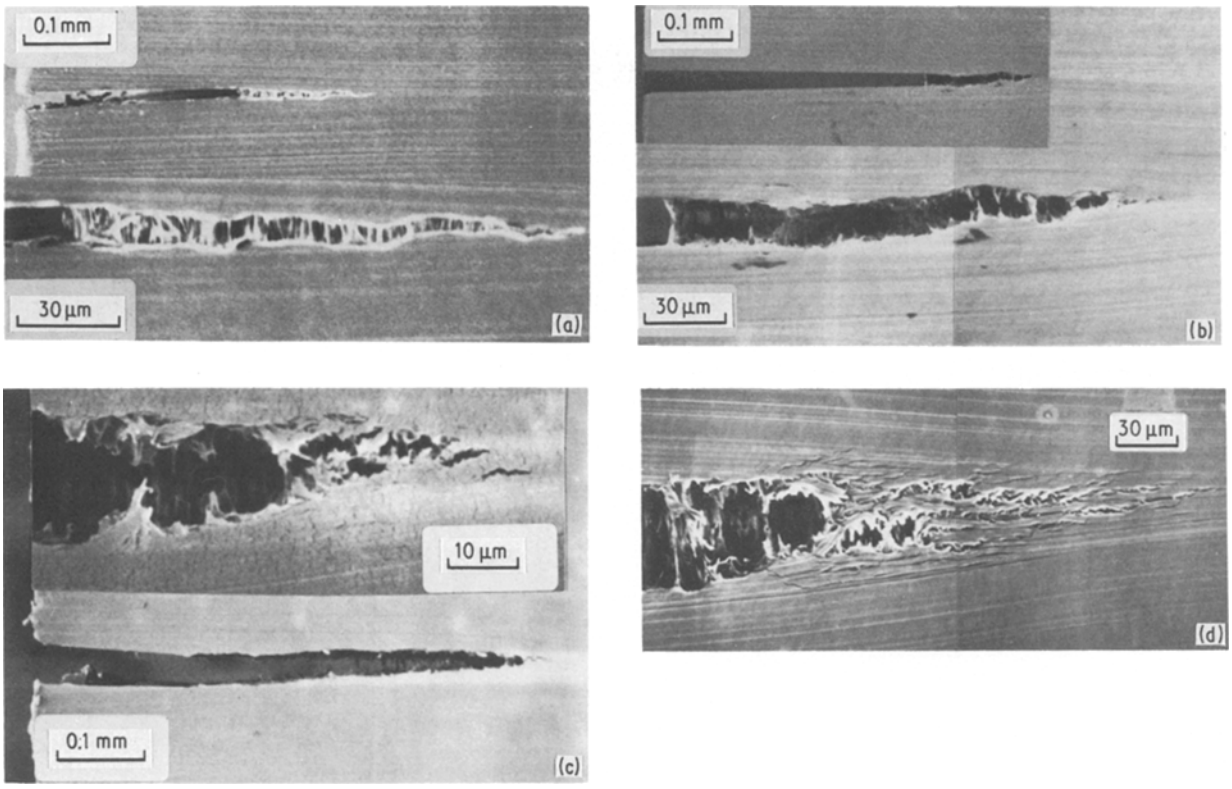

Figure 3 Crack tip damage of samples with different loading conditions. (a) a_0 = 0.263 mm, σ = 10 MPa, 42° C, loading time = 215 min, COD = 19.2 μm, α = 7°. (b) a_0 = 0.419 mm, σ = 10 MPa, 30° C, loading time = 555 min, COD = 25.8 μm, α = 8°. (c) a_0 = 0.188 mm, σ = 10 MPa, 42° C, loading time = 420 min, COD = 50.9 μm, α = 9°. (d) a_0 = 277 mm, σ = 12 MPa, 42° C, loading time = 367 min, COD = 334 μm, α = 15°.

crack growth in polymers that has been reported in the literature.

3.4. The initial rate, $\dot{\delta}_0$ against stress and notch depth

Fig. 7 at 42° C shows log $\dot{\delta}_0$–log stress at a constant a_0. The resulting equation is given by

$$\dot{\delta}_0 = C_1\sigma^{5.4} \quad (4)$$

where C_1 depends on a_0 and T. The experimental scatter in the exponent ranged from 5.2 to 5.5 with a correlation coefficient of 0.98.

Fig. 8 shows log $\dot{\delta}_0$–log a_0 for a constant stress where

$$\dot{\delta}_0 = C_2a_0^{1.8} \quad (5)$$

with a correlation coefficient ranging from 0.93 to 0.98. Combining Equations 4 and 5

$$\dot{\delta}_0 = 1 \times 10^{-11}\sigma^{5.4}a_0^{1.8} \quad \mu\text{m min}^{-1} \quad (6)$$

where a_0 is in micrometres, σ in MPa, and T = 42° C.

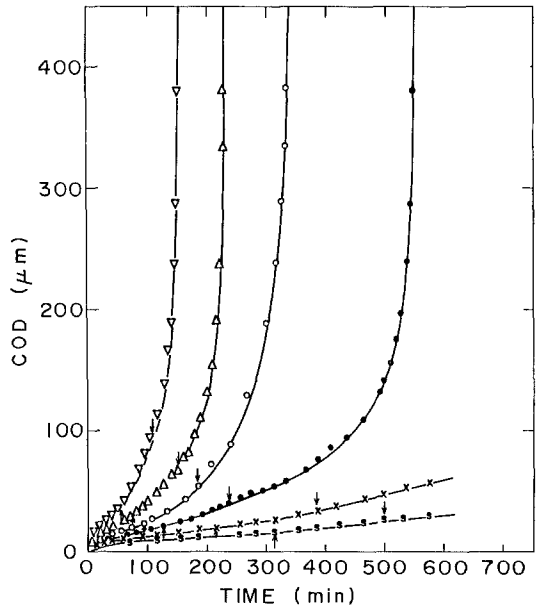

Figure 4 Crack opening displacement, COD, against time for various stresses at a nearly constant notch depth of 0.40 mm and 42° C. (s) 7.56, 0.4; (x) 8, 0.428; (●) 9, 0.387; (○) 10, 0.396; (△) 11, 0.4; (▽) 12, 0.415 stress (MPa), a_0(mm).

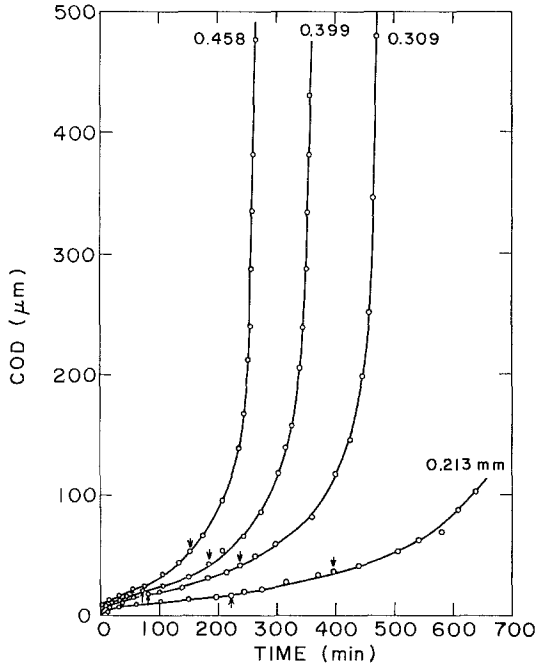

Figure 5 Same as Fig. 4 except for various notch depths and a constant stress of 10 MPa and 42° C.

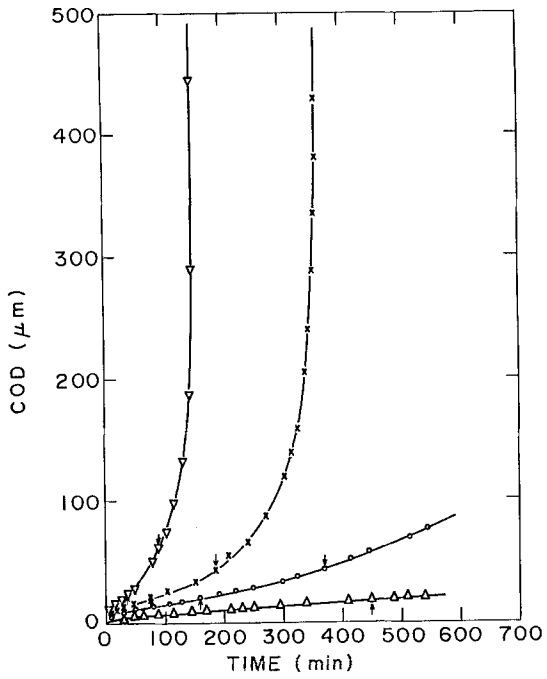

Figure 6 Same as Fig. 5 except for various temperatures and a nearly constant notch depth of 0.40 mm and 10 MPa. (△) 30, 0.397; (○) 36, 0.400; (×) 42, 0.402; (▽) 48, 0.418 temperature (° C), a_0(mm).

The stress intensity for three-point bending is given by [6]

$$K = \frac{3PS(a)^{1/2}}{2BW^2} Y_1(a/W) \text{ for } S/W = 8,$$

$$Y_1(a/W) = 1.96 - 2.75(a/W) + 13.66(a/W)^2 - 23.98(a/W)^3 + 25.22(a/W)^4 \quad (7)$$

where P is load, S, B, and W are span of supports, width and thickness of sample. Fig. 9 shows log $\dot{\delta}_0$ against log K_0 at 42° C where K_0, the initial stress intensity (Equation 7) is in MPa m$^{1/2}$.

$$\dot{\delta}_0 = 17K_0^{4.5} \quad \mu\text{m min}^{-1} \quad (8)$$

The correlation coefficient is 0.98 for 29 tests. It is

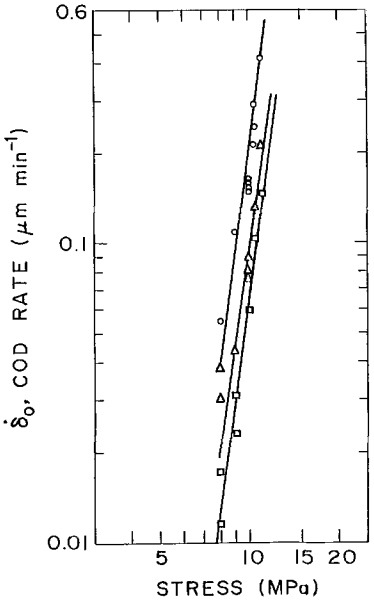

Figure 7 Log $\dot{\delta}_0$ (initial damage rate)–log σ at a constant notch depth. (○) 0.40; (△) 0.30; (□) 0.20 mm = a_0, 42° C.

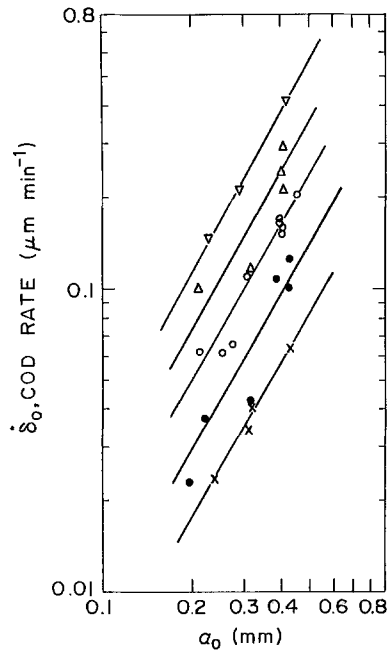

Figure 8 Log $\dot{\delta}_0$–log a_0 at a constant stress. (×) 8; (●) 9; (○) 10; (△) 11; (▽) 12, stress (MPa), 42° C.

expected that the exponent for K_0 be less than the exponent for stress in Equation 6 because the exponent for a_0 in Equation 6 is less than one-half the exponent for stress. However Equation 6 is more detailed than Equation 8 and should be the best basis for constructing theoretical models. At times Equation 8 may be more convenient for discussing the combined effects of stress and notch depth. There is an inconsistency between Equations 6 and 8, since $5.4 \neq 2 \times 1.8$, which is obscured by the log–log method of plotting in spite of the high correlation coefficients for both plots.

3.5. Relationship of crack growth to the initiating stage

As shown in a previous paper [3], the shape of a δ–t curve beyond the linear region can be predicted from

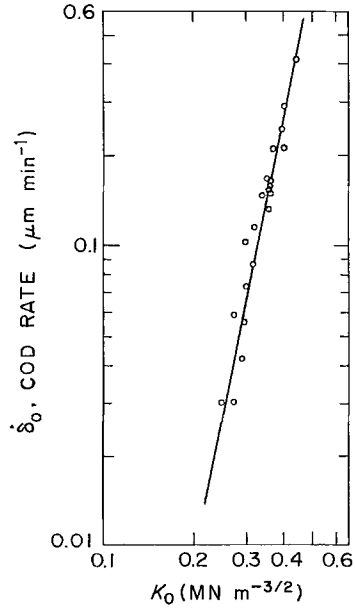

Figure 9 Log $\dot{\delta}_0$–log K_0, the initial stress intensity at 42° C.

TABLE I Shows reproducibility of $\dot{\delta}_0$

Test conditions				$\dot{\delta}_0$		$\dot{\delta}_0$	
a_0 (μm)	σ (MPa)	T(°C)	K_0 (MN m$^{-3/2}$)	(experimental value) (μm min^{-1})	Scatter	Normalized to same a_0 (μm min^{-1})	Scatter after normalization
396	10	42	0.358	0.17		0.16	
406	10	42	0.363	0.16		0.16	
399	10	42	0.360	0.16	±12%	0.16	±4%
402	10	42	0.360	0.15		0.15	
458	10	42	0.385	0.20		0.15	
429	10	36	0.373	6.3×10^{-2}		5.2×10^{-2}	
400	10	36	0.360	8.4×10^{-2}	±18%	8.1×10^{-2}	±20%
393	10	36	0.357	5.5×10^{-2}		5.5×10^{-2}	
393	10	36	0.357	6.7×10^{-2}		6.7×10^{-2}	
400	11	42	0.396	0.24		0.25	
409	11	42	0.400	0.22	±16%	0.22	±17%
404	11	42	0.398	0.30		0.31	
387	9	42	0.319	0.11		0.134	
428	9	42	0.335	0.13	±11%	0.125	±5%
307	8	42	0.254	3.4×10^{-2}		3.4×10^{-2}	
307	8	42	0.254	4.0×10^{-2}	±11%	4.0×10^{-2}	±11%
280	10	42	0.304	6.5×10^{-2}		5.8×10^{-2}	
254	10	42	0.296	6.2×10^{-2}	±4%	6.2×10^{-2}	±4%
465	10	30	0.388	3.7×10^{-2}		2.5×10^{-2}	
397	10	30	0.357	2.8×10^{-2}	±20%	2.8×10^{-2}	±7%
				Average error	±14%	Average error	±9%

Used $\dot{\delta}_0 = 17 K_0^{4.5}$ to normalize the $\dot{\delta}_0$ values.

its initial slope $\dot{\delta}_0$. In the case of three-point bending the prediction holds from about 20 to 200 μm. The slope at time t, $\dot{\delta}$, should be related to $\dot{\delta}_0$ by the following equation if Equations 6 and 8 hold during crack growth and if a_0 is replaced by the instantaneous crack length.

$$\frac{\dot{\delta}}{\dot{\delta}_0} = \left(\frac{a_0 + \delta/\alpha}{a_0 + \delta_c/\alpha}\right)^m \tag{9}$$

where m is expected to be about 2 or one-half the exponent for K in Equation 8.

In Fig. 10 log $(\dot{\delta}/\dot{\delta}_0)$ is plotted in accordance with Equation 9 where $\delta_c = 20\,\mu$m and $\alpha = 0.14$ rad. The points in Fig. 10 represent about 7 values of $\dot{\delta}$ per

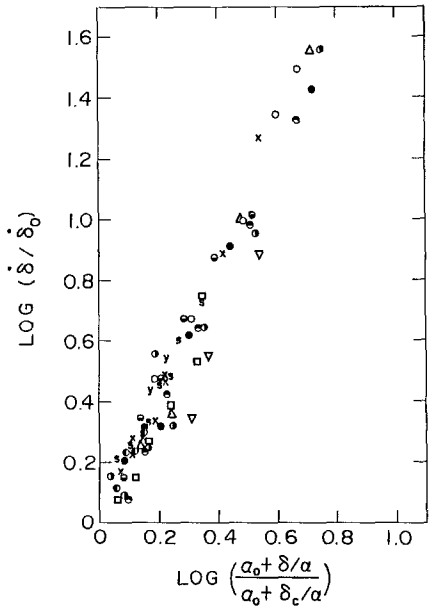

Figure 10 Plot of Equation 9. (○) 10, 406; (x) 9, 387; (△) 12, 415; (●) 11, 400; (◐) 8, 428; (◑) 12, 290; (◓) 11, 315; (◒) 10, 309; (y) 9, 317; (▽) 12, 231; (□) 11, 208; (s) 10, 213; stress (MPa), a_0(μm).

curve using about 12 representative δ–t curves. The resulting value for m is 2.0 with a correlation coefficient of 0.97 whereas Equations 6 and 8 predict a value between 1.8 and 2.2. This result shows that the rate of crack growth is related to the initial rate of damage, $\dot{\delta}_0$, times the increasing stress intensity factor as the crack grows.

3.6. Dependence of crack growth rate on K

The crack growth rate, $\dot{a}$, is related to $\dot{\delta}$ through Equation 2. Thus by taking the slope of the δ–t curve $\dot{a}$ is obtained as a function of K where the instantaneous crack length, a, is

$$a = a_0 + \delta/\alpha \tag{10}$$

Since σ is constant, the instantaneous value of stress intensity, K, can be obtained by inserting a from Equation 10 into the formula for K. The plot of log $\dot{\delta}$–log K at 42° C is shown in Fig. 11 where

$$\dot{\delta} = 6K^{4.5} \quad \mu\text{m min}^{-1} \tag{11}$$

The value of the exponent in Equation 11 is the same as in Equation 8, and its front factor, 6, is expected to be equal to $(a_0/(a_0 + \delta_c/\alpha))^2$ times the front factor 17 in Equation 8. For the range of a_0 used in this investigation the front factor in Equation 11 is calculated to be 8 which is close to the observed value of 6 in Equation 11. Thus Equations 8, 9 and 11 are self-consistent.

3.7. Dependence of $\dot{\delta}_0$ on temperature

The previous results are all for 42° C. Fig. 12 shows log $\dot{\delta}_0$–$1/T$. The resulting activation energy is 110 kJ mol^{-1}. This is about the same value as obtained by Chan and Williams [7, 8] and from our previous investigation in tension on the same polyethylene [3]. A 1° C change at 30° C produces a 16% change in the

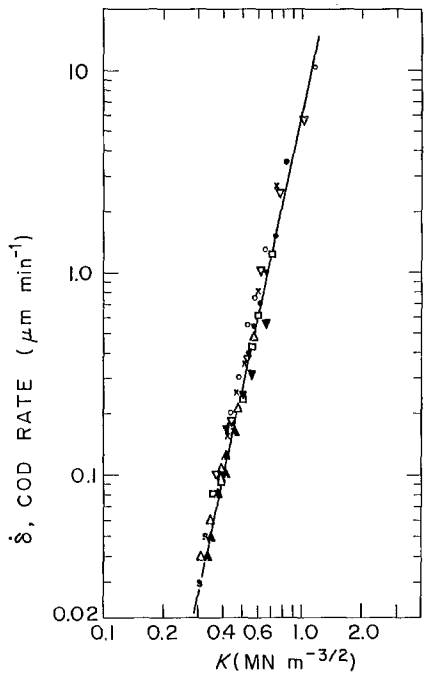

Figure 11 Log $\dot{\delta}$, instantaneous rate of damage–log K, the instantaneous stress intensity. (s) 400, 7.56; (▽) 387, 9; (△) 317, 9; (○) 458, 10; (x) 309, 10; (▲) 213, 10; (□) 208, 11; (●) 415, 12; (▼) 231, 12; a_0(μm), σ (MPa). At 42° C.

damage rate. Using the activation energy of 110 kJ mol^{-1}, the following equation is obtained in conjunction with Equation 6

$$\dot{\delta}_0 = 17 \times 10^6 e^{-Q/RT} \sigma^{5.4} a_0^{1.8} \quad \mu m\,min^{-1} \quad (12)$$

where $Q = 110\,kJ\,mol^{-1}$, σ is in MPa and a_0 is in μm. This equation summarizes the effects of T, σ and a_0 over the range of 30 to 48° C, 7.5 to 12 MPa, and a_0 = 200 to 450 μm.

3.8. Predicting time to failure

In a previous paper [3] with single edge notched tension specimens it was shown that the time to failure t_f could be predicted from $\dot{\delta}_0$, α, a_0 and δ_c where $t_f = (\alpha a_0 + \delta_c)/\dot{\delta}_0$. In the present investigation the best prediction of failure time, t_f, was obtained from the equation

$$t_f(\text{theor}) = \alpha a_0/\dot{\delta}_0 \quad (13)$$

Table II shows the comparison of Equation 13 with the experimental values using an average value of α = 0.14 rad. The average error between Equation 13 and the experimental value of t_f is ± 20% based on 16 tests. This degree of prediction is excellent for this type of fracture test.

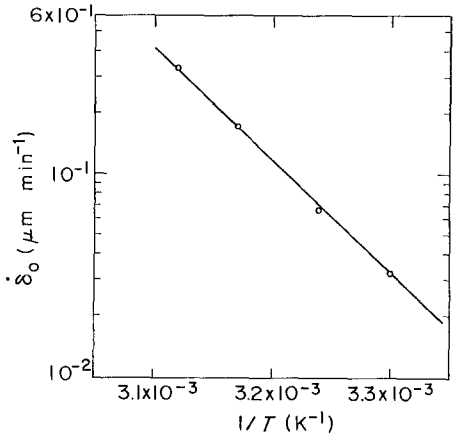

Figure 12 Plot of log $\dot{\delta}_0$–$1/T(K^{-1})$. a_0 = 400 μm; σ = 10 MPa.

4. Discussion

4.1. Reproducibility of data

By carefully controlling the experimental variables, notch depth, stress and temperature and by special processing of the material during compression moulding it is now possible to reproduce the initial velocity of damage to within an error of about ± 20%. This is important because the subsequent course of crack growth and time to failure depend mostly on the initial velocity of the damaged zone that emanates from the notch.

TABLE II Comparison of theoretical and experimental times for failure

a_0 (μm)	σ (MPa)	$\dot{\delta}_0$ (μm min^{-1})	t_f (theo) (min)	t_f (expt) (min)	$\frac{t_f\,(\text{expt})}{t_f\,(\text{theo})}$
387	9	0.11	493	555	1.13
396	10	0.17	326	335	1.03
400	11	0.24	233	233	1.00
415	12	0.44	132	155	1.17
290	12	0.20	203	327	1.61
315	11	0.14	315	426	1.35
309	10	0.11	393	473	1.20
239	8	0.02	1673	1920	1.15
409	11	0.22	260	253	0.97
404	11	0.30	189	220	1.16
406	10	0.16	355	336	0.95
399	10	0.16	349	362	1.04
402	10	0.15	375	291	0.78
396	10	0.17	326	386	1.18
428	9	0.13	461	449	0.97
458	10	0.20	321	265	0.83
				Average = 1.10 ± 0.20	

$t_f(\text{theo}) = \alpha a_0/\dot{\delta}_0$.
α = angle of damage zone, 8°.
a_0 = initial notch depth.
$\dot{\delta}_0$ = initial slope of δ–t curve.

4.2. General shape of the damaged zone

This paper generally emphasized the regime of stress that was less than about one-half the yield point because higher stresses produced a balloon-shaped damaged zone whereas the lower stresses produce a thin triangular damaged zone that is characteristic of the long time brittle failure found in PE (Fig. 3). By measuring both the notch opening at the surface and at its root, the apex angle of the damaged zone was determined and found to be about 8° during the initial stage of growth. Knowing this angle, the length of the damaged zone is directly related to the notch opening at its root. The size and shape of the damaged zone that is observed shortly after loading the specimen is about that predicited by the Dugdale theory.

A critical opening displacement of the damaged zone was observed, beyond which the $\delta - t$ curve began to accelerate markedly, and it signals the beginning of true crack growth. Prior to this critical opening displacement, which was about 15 to 25 μm, the damage zone extended by the growth of microcrazes within it while maintaining a constant apex angle of about 8°.

4.3. The initial damage rate

The initial damage rate $\dot{\delta}_0$ is the most significant parameter since it determines the subsequent kinetics of crack growth (Equation 9) and also the time to fracture (Equation 13). Equation 12 is the basis for predicting the crack growth and time to failure in terms of the initial conditions of T, σ and a_0. Thus, theoretical modelling of slow crack growth failure in PE must be consistent with Equation 12 and use the microscopic observations that the damaged zone grows by the growth of microcrazes within it.

4.4. Other theories

Kinloch [9] described the damage rate in a polymer in terms of a single craze growing from a crack. He modified the Dugdale equation by assuming that the yield point decreased with time and thereby caused the damage zone to grow. The Kinloch theory essentially predicts that $\dot{\delta}_0$ should vary as K^2 whereas Equation 8 shows $\dot{\delta}_0$ varies as $K^{4.5}$. For PE the damaged zone does not consist of a single craze.

Chan and Williams [7, 8] measured a crack growth rate in the same PE as ours and found that is varied as K^4. Considering the amount of scatter in their data, their results are in agreement with our observations. Chan and Williams [7, 8] suggested that the K^4 dependence of crack growth comes from the nucleation of voids and a diffusion process between the voids in the damaged zone. Their theory has the merit of postulating growth of microcracks which we have observed experimentally but otherwise has little experimental support.

In metals there are many theories involving the initiation of crack growth, by the stress controlled diffusion during the growth of microvoids. A representative theory by Vitek [10] and Wilkinson [11] starts with the stress field generated by a notch which then is modified by the subsequent growth of a plastic zone. Under this stress field, voids grows at a rate which involves the diffusion of vacancies. Ultimately the vacancies grow to form a true crack. The predicted dependence of the damage rate on K depends on the power law used for the creep function and on other factors which are not readily explainable.

4.5. Our theory

The theory starts with the microscopic observation that the damaged zone consists of a triangular area A where

$$A = \frac{\delta^2}{2\alpha} \tag{14}$$

δ is the notch opening displacement. The micrographs show that there are microcrazes within the damaged zone and as these microcrazes increase in area so does the damaged zone. Thus the rate of increase in area of damaged zone may be described by

$$\dot{A} = N\dot{A}_c \tag{15}$$

where $\dot{A} = \delta\dot{\delta}/\alpha$; N is the number of microcrazes and $\dot{A}_c$ is the average rate of increase in area of a microcraze. It is now assumed that N microcrazes are nucleated when the specimen is first loaded so that

$$N = \frac{\delta_0^2 \varrho}{2\alpha} \tag{16}$$

where δ_0 is the COD immediately after loading and ϱ is the density of microcrazes per unit area. The area of a microcraze is irregular but in general we can say that

$$A_c = \beta b^2 \tag{17}$$

so that $\dot{A}_c = 2\beta b\dot{b}$; β is a shape factor, b is a dimension of the microcraze and $\dot{b}$ is rate of opening of a microcraze. Combining Equations 14 to 17

$$\dot{\delta} = \delta_0^2 \varrho \left(\frac{b}{\delta}\right) \dot{b}\beta \tag{18}$$

The experimental data show that $\dot{\delta}$ is constant during the initial stage. Thus, all the factors in Equation 18 must combine so that their product does not depend on time. Let us examine the expected behaviour of each factor. ϱ is expected to depend on the spectrum of sites from which microcrazes may nucleate and on the stress required to nucleate a particular site. Probably the initial stress field that occurs during loading is mainly responsible for ϱ so that it depends on K_0, the initial stress intensity. After the microvoids form, the local stress relaxes so that additional microvoids are not likely to be nucleated. Under constant stress the craze density is expected to increase with time, but after the stress relaxes the number of crazes is expected to be constant because the stress has a much greater effect on craze density than time. Initially

$$\delta = \delta_0 + \dot{\delta}_0 t \tag{19}$$

If $\dot{b}$ = constant during the initial stage then

$$b = b_0 + \dot{b}t \tag{20}$$

where b_0 is the microvoid size at $t = 0$. In the range where $\delta_0 < \delta$ and $b_0 < b$, combining Equations 18, 19 and 20 gives

$$\dot{\delta}_0 \approx \delta_0 \dot{b} \varrho^{1/2} \beta^{1/2} \tag{21}$$

The dependence of $\dot{b}$ on stress and a_0 is not known. However the temperature dependence of $\dot{\delta}_0$ is primarily determined by the temperature dependence of $\dot{b}$. The insertion of Equation 3 in Equation 21 gives

$$\dot{\delta}_0 = \frac{K^2 \dot{b} \varrho^{1/2} \beta_{1/2}}{\sigma_y E(1 - \nu^2)} \quad (22)$$

when this equation is compared with the experimental results in Equation 8, it is suggested that

$$(\dot{b}\varrho^{1/2}) \propto K^{2.5}$$

The above relationship can be verified experimentally by quantitative microscopic measurements of $\dot{b}$ and ϱ as a function of K.

5. Summary

1. By carefully controlling the notch depth, stress and moulding conditions, it is now possible to control the accuracy of measurements of slow crack growth in PE to within $\pm 20\%$.

2. The quantitative dependence of the initial damage rate on stress, notch depth, and temperature have been determined under plane strain conditions and three-point bending.

3. The initial rate of damage begins to accelerate at a critical crack opening displacement of about 20 μm.

4. From the critical crack opening displacement and the initial slope of the damage–time curve, the subsequent course of crack growth and ultimate fracture time can be predicted.

5. The basic mechanism for growth of the damaged zone comes from the growth of microcrazes within it.

Acknowledgements

The research was supported by the Department of Energy. Use was made of the Central Facilities of the Materials Research Laboratory at the University of Pennyslvania which is supported by the National Science Foundation. The authors are also indebted to colleagues E. Anderson and X. Q. Wang for their technical help.

Stimulation and support was provided by the general research programme of the Gas Research Institute for the purpose of enhancing the utilization of polyethylene pipe lines.

Our thanks to Dr D. J. van Dijk from the Dutch Plastics and Rubber Research Institute in Delft who told us about the moulding technique.

References

1. S. K. BHATTACHARYA and N. BROWN, *J. Mater. Sci.* **19** (1984) 2519.
2. *Idem, ibid.* **20** (1985) 2767.
3. X. LU and N. BROWN, *J. Mater. Sci.* **21** (1986) 2423.
4. D. J. VAN DIJK, private communication from Dutch Rubber and Plastic Institute Delft (1984).
5. B. MELVE, thesis, Norwegian Institute of Technology (1985).
6. W. F. BROWN Jr and J. E. SRAWLEY, ASTM STP 410 (American Society for Testing and Materials, Philadelphia, Pennsylvania, 1969).
7. M. K. V. CHAN and J. G. WILLIAMS, *Polymer* **24** (1983) 254.
8. J. G. WILLIAMS, "Fracture Mechanics of Polymers" (Wiley, New York, 1984) p. 209.
9. A. J. KINLOCH, *Met. Sci.* **14** (1980) 305.
10. V. VITEK, *Acta Metall.* **26** (1978) 1345.
11. D. S. WILKINSON and V. VITEK, *ibid.* **30** (1982) 1723.

Received 30 December 1985
and accepted 11 February 1986